Cauchy-perturbative matching reexamined: Tests in spherical symmetry

Burkhard Zink,[1,*] Enrique Pazos,[2,3,4,†] Peter Diener,[2,3,‡] and Manuel Tiglio[2,3,§]

[1]*Max-Planck-Institut für Astrophysik, Karl-Schwarzschild-Str. 1, 85741 Garching bei München, Germany*
[2]*Department of Physics and Astronomy, 202 Nicholson Hall, Louisana State University, Baton Rouge, Louisiana 70803, USA*
[3]*Center for Computation and Technology, 302 Johnston Hall, Louisana State University, Baton Rouge, Louisiana 70803, USA*
[4]*Departamento de Matemática, Universidad de San Carlos de Guatemala, Edificio T4, Facultad de Ingeniería,*
Ciudad Universitaria Z. 12, Guatemala

During the last few years progress has been made on several fronts making it possible to revisit Cauchy-perturbative matching (CPM) in numerical relativity in a more robust and accurate way. This paper is the first in a series where we plan to analyze CPM in the light of these new results. One of the new developments is an understanding of how to impose constraint-preserving boundary conditions (CPBC); though most of the related research has been driven by outer boundaries, one can use them for matching interface boundaries as well. Another front is related to numerically stable evolutions using multiple patches, which in the context of CPM allows the matching to be performed on a spherical surface, thus avoiding interpolations between Cartesian and spherical grids. One way of achieving stability for such schemes of arbitrary high order is through the use of penalty techniques and discrete derivatives satisfying summation by parts (SBP). Recently, new, very efficient and high-order accurate derivatives satisfying SBP and associated dissipation operators have been constructed. Here we start by testing all these techniques applied to CPM in a setting that is simple enough to study all the ingredients in great detail: Einstein's equations in spherical symmetry, describing a black hole coupled to a massless scalar field. We show that with the techniques described above, the errors introduced by Cauchy-perturbative matching are very small, and that very long-term and accurate CPM evolutions can be achieved. Our tests include the accretion and ring-down phase of a Schwarzschild black hole with CPM, where we find that the discrete evolution introduces, with a low spatial resolution of $\Delta r = M/10$, an error of 0.3% after an evolution time of $1,000,000M$. For a black hole of solar mass, this corresponds to approximately $5s$, and is therefore at the lower end of timescales discussed e.g. in the collapsar model of gamma-ray burst engines.

I. INTRODUCTION

It is generally expected that the geometry of compact sources should resemble flat spacetime at large enough distances. This is true not only qualitatively, but through very precise falloff conditions that are built into the formal definition of asymptotic flatness. Within this definition, the deviations from flat spacetime are well described (in the sense of the leading order behavior of an expansion in powers of ''$1/r$'') by perturbations of the Schwarzschild spacetime [1].

Such perturbations can in turn be studied through the gauge invariant Regge-Wheeler and Zerilli (RWZ) formalisms [2,3]. These allow one to derive, after a spherical harmonic decomposition (that is, for each ''(ℓ, m)''), two master evolution equations for the truly gauge invariant, linearized physical degrees of freedom. Because of the multipole decomposition, these equations involve only one spatial coordinate (the radial one). The fact that they are one-dimensional implies that these master equations

can be solved for very large computational domains with very modest computational resources. On the other hand, three-dimensional Cauchy codes are very demanding on their resource requirements. Even though mesh refinement can help in this respect, there is a limit to how much one can coarsen the grid in the asymptotic region; this limit is set by the resolution required to reasonably represent wave propagation in the radiative zone. The use of a grid structure adapted to the physical geometry (possibly through multiple patches) can also help [4–6], but one still ends up imposing artificial (even if constraint-preserving) boundary conditions at the outer boundary. For example, one in general misses information about the geometry outside the domain [7].

Two approaches that at the same time provide wave extraction, physically motivated boundary conditions, and extend the computational domain to the radiative regime are Cauchy-characteristic [8–10] and Cauchy-perturbative matching (CPM) [11–14]; this paper is concerned with the latter. The idea is to match at each timestep a fully nonlinear Cauchy code to an outer one solving, say, the RWZ equations.[1]

---

*Electronic address: bzink@mpa-garching.mpg.de
†Electronic address: enrique@cct.lsu.edu
‡Electronic address: diener@cct.lsu.edu;
Web address: http://www.cct.lsu.edu
§Electronic address: tiglio@cct.lsu.edu;
Web address: http://www.cct.lsu.edu

---

[1]Even though including the angular momentum of the background is a high-order correction in terms of powers of $1/r$, one might, in principle, try to solve for perturbations of Kerr spacetime (as opposed to Schwarzschild).

This paper is the first one in a series where we plan to revisit CPM in the light of some recent technical developments—which we describe below—that should help in its implementation. Before discussing these developments, we point out and summarize some features present in the original implementation of CPM which we hope to improve on:

(1) The nonlinear Cauchy equations were solved on a Cartesian, cubic grid. On the other hand, the RWZ equations use a radial coordinate for the spatial dimension. Mixing Cartesian coordinates with spherical ones leads to the need for interpolating back and forth between both grids. Especially when using high-order methods, this type of interpolation might not only be complicated but also subtle: depending on how it is done it might introduce noise and sometimes it might even be a source of numerical instabilities.

(2) When injecting data from the perturbative module to the Cauchy code and vice versa boundary conditions were given to all modes, irrespectively of their propagation speed, and without taking into account the existence of constraint violating boundary modes. One would intuitively expect a cleaner matching if boundary conditions are given according to the characteristic (propagation) speeds of the different modes, and even cleaner if constraint-preservation is automatically built in during the matching.

(3) Low order numerical schemes, which result in slow convergence, were used.

In recent years there has been progress on several related fronts that should in principle help in the implementation of CPM. We describe these new results next[2]:

(1) The first improvement is the ability to implement smooth (in particular, spherical) boundaries in $3D$ Cauchy evolutions [4–6]. One important advantage of this is the fact that the matching can be performed—to either a perturbative or a characteristic outer module—without the need for interpolation between spherical and Cartesian grids. In that way a possible source of noise can be eliminated. It is now understood how to match different domains using schemes of arbitrary high order while at the same time ensuring numerical stability. One way of doing so is through the use of multiple patches (much in the same way multiple charts are used in differential geometry), penalty terms and difference operators satisfying summa-

tion by parts [4] (more about this below). This is the approach we shall explore here in the context of CPM.[3]

(2) The second improvement is the construction of constraint-preserving boundary conditions (CPBC). Several efforts have by now reported numerically stable (in the sense of convergent) implementations of such boundary conditions for the fully three-dimensional nonlinear Einstein's equations [16–18]. Furthermore, there have been reports in the context of three-dimensional Cauchy-characteristic matching that significant improvements are obtained when this type of boundary conditions are used [18]. With this in mind, we will test their use in CPM.

(3) Lastly, new, accurate and efficient high-order difference operators satisfying SBP and associated dissipative operators have been constructed recently [19–22]. As mentioned above, in conjunction with certain penalty interface treatment such operators guarantee numerical stability when "glueing" together different computational grids. We will test these operators in the context of CPM.

We have incorporated these techniques, i.e., high-order summation-by-parts finite differencing and dissipation operators, multiple coordinate patches with penalty interpatch constraint-preserving boundary conditions and Cauchy-perturbative matching, into a spherically symmetric numerical code evolving the Einstein-Christoffel form of the field equations [23], minimally coupled to a Klein-Gordon field. Using this tool, we can test the performance of the numerical methods in a nontrivial, but easily reproducible and computationally inexpensive setting, and gain experience for three-dimensional applications. The evolutions presented here model black holes with excision in isolation, under dynamical slicings, and black holes accreting scalar field pulses, which are used as a scalar analogue of gravitational radiation.

The plan of this paper is as follows. In Sec. II we introduce the continuum system and the numerical techniques we have used. Results are presented in Sec. III, where a black hole is evolved successively from simple settings, i.e., single-patch, isolated, Killing-field adapted gauges, to more involved ones including Cauchy-perturbative matching and scalar pulse accretion. Finally, in Sec. IV, we draw conclusions and give an outlook to future work.

---

[2]There is actually another ingredient: the use of a generalized perturbative formalism that allows for any (spherically symmetric) slicing of the background Schwarzschild metric [15]. However, since such ingredient will not appear in the simplified model that we look at in this paper, we skip its discussion here.

[3]Regardless of whether matching is present or not, the use of multiple coordinate patches has advantages when modelling black holes through excision of the singularity from the computational domain.

II. EQUATIONS AND METHODS

A. Evolution equations and constraint-preserving boundary conditions

In this paper we use the Einstein-Christoffel (EC) system [23] in spherical symmetry. We follow the notation of Ref. [24];, in particular, the densitized lapse is denoted by $\alpha = N g^{-1/2}$, and $\tilde{\alpha} = \alpha r^2 \sin(\theta)$ is introduced for convenience. Here, g is the determinant of the 3-metric and N the lapse function, while the 4-metric is written as

$$ds^2 = -N^2 dt^2 + g_{rr}(dr + \beta dt)^2$$
$$+ r^2 g_T(d\theta^2 + \sin^2\theta d\phi^2)$$

The vacuum part of the evolution equations in spherical symmetry for this formulation constitute a symmetric hyperbolic system of six first-order differential equations. The vacuum variables are the two metric and extrinsic curvature components

$$g_{rr}, \qquad g_T, \qquad K_{rr}, \qquad K_T,$$

where the extrinsic curvature is written as

$$K_{ij} = K_{rr}dr^2 + r^2 K_T(d\theta^2 + \sin^2\theta d\phi^2),$$

plus two auxiliary variables needed to make Einstein's equations a first-order system. These extra variables are defined as

$$f_{rrr} = \frac{g_{rr}'}{2} + 4\frac{g_{rr}f_{rT}}{g_T}, \qquad f_{rT} = \frac{g_T'}{2} + \frac{g_T}{r}.$$

In addition, a massless Klein-Gordon field is minimally coupled to the geometry [6,25]. The scalar field equation

$$g^{ab}\nabla_a\nabla_b\Psi = 0$$

is converted into a first-order system by introduction of the variables

$$\Pi = \frac{1}{N}(\beta\Psi' - \dot{\Psi}), \qquad \Phi = \Psi'.$$

Throughout this paper the "prime" and "dot" represent partial derivatives with respect to r and t, respectively.

Constraint-preserving boundary conditions are imposed by analyzing the characteristic modes of the main and constraint evolution systems, as discussed in [25]. These modes and their associated characteristic speeds are summarized in Table I. For illustration purposes, we also show the direction of propagation of each mode in the Schwarzschild spacetime in Painlevé-Gullstrand coordinates [26–28].

From Table I we notice that for the Schwarzschild spacetime there are four ingoing and two outgoing gravitational modes at the outer boundary, and therefore expect the same count to hold for perturbations thereof. Boundary conditions for the incoming modes u_1, u_2 and u_4 are fixed by the

TABLE I. Characteristic modes of the Einstein-Christoffel system in spherical symmetry, and their direction of propagation for a Schwarzschild spacetime in Painlevé-Gullstrand coordinates with respect to the vector field ∂_r. In this gauge, all modes are outflow at the inner boundary, if it is located at $r < 2M$, while boundary conditions have to be applied to the incoming modes u_1, u_2, u_3, u_4 and u_8 at the outer boundary, assuming it is located at $r > 2M$.

Mode	Speed	$r < 2M$	$r > 2M$
$u_1 = g_{rr}$	β	left	left
$u_2 = g_T$	β	left	left
$u_3 = K_{rr} - f_{rrr}g_{rr}^{-1/2}$	$\beta + \tilde{\alpha}g_T$	left	left
$u_4 = K_T - f_{rT}g_{rr}^{-1/2}$	$\beta + \tilde{\alpha}g_T$	left	left
$u_5 = K_{rr} + f_{rrr}g_{rr}^{-1/2}$	$\beta - \tilde{\alpha}g_T$	left	right
$u_6 = K_T + f_{rT}g_{rr}^{-1/2}$	$\beta - \tilde{\alpha}g_T$	left	right
$u_7 = \Pi + \Phi g_{rr}^{-1/2}$	$\beta - \tilde{\alpha}g_T$	left	right
$u_8 = \Pi - \Phi g_{rr}^{-1/2}$	$\beta + \tilde{\alpha}g_T$	left	left

CPBC procedure. Thus, the only free incoming modes are u_3, which represents a gauge mode and u_8, which represents a physical one (see [25] for more details). Boundary conditions do not need to be specified at the inner boundary if it is located inside the event horizon, because all modes are outflow there.

B. Cauchy-perturbative matching

Since there is no radiative degree of freedom in spherically symmetric spacetimes, we use the massless Klein-Gordon field as a scalar analogue of gravitational waves. To emulate the setup of three-dimensional Cauchy-perturbative matching as closely as possible, the scalar wave is evolved on a fixed Schwarzschild background in a "perturbative" patch defined for $r \geq r_m$, while the fully nonlinear Einstein's equations are evolved in the "Cauchy" patch, defined for $r \in [r_e, r_m]$, where r_e and r_m denotes the excision radius and the matching radius, respectively.

The fact that we are using CPBC allows us to perform a clean matching. From the analytical point of view our matching works in the following way: As mentioned above, after the CPBC procedure, only two free characteristic modes are entering the Cauchy computational domain (at $r = r_m$), denoted by u_3 and u_8. Since in a very precise sense u_3 is a gauge mode, we are free to give boundary conditions to it in a very simple way: we just set it to its initial value. Regarding u_8, we use the perturbative value of the same quantity coming from the perturtative domain as counterpart, and communicate these two modes (how this is done at the numerical level is explained below). Similarly, there is only one characteristic mode entering the perturbative domain, which is the linearized version of u_7. We therefore communicate the nonlinear and linear versions of that mode as well.

C. Discrete techniques

Given a well-posed initial-boundary value problem for Einstein's field equations, we construct a stable and accurate discrete system by using operators satisfying the SBP property. In short, a finite difference operator, D, satisfies SBP on a computational domain $[a, b]$ discretized using grid points $i = 1, \ldots, n$ and a grid spacing h if

$$\langle u, Dv \rangle + \langle v, Du \rangle = (uv)|_a^b \qquad (1)$$

holds for all grid functions u, v. Here the scalar product, Σ is defined in terms of its coefficients σ_{ij} by

$$\langle u, v \rangle = h \sum_{i,j=1}^{n} u_i v_j \sigma_{ij}. \qquad (2)$$

In this paper we use the new, efficient, and accurate high-order SBP difference operators and associated dissipation operators constructed in Ref. [22]. Thus, as mentioned, this paper also serves as an extra test of those new operators.

SBP operators are standard centered finite difference operators in the interior of the domain, but the stencils are modified to yield lower order operators in a region close to the boundaries (at the boundary itself the stencil is completely one sided). There are several types of SBP operators depending on the properties of the norm. The simplest are the diagonal norm operators. They have the advantage that SBP is guaranteed to hold in several dimensions by simply applying the $1D$ operator along each direction and that numerical stability can be guaranteed by discrete energy estimates in a wide range of cases. The main disadvantage is that the order of the operator at and close to the boundary is only half the interior order. We denote the SBP operators by the interior and boundary order and consider here the diagonal operators D_{2-1}, D_{4-2}, D_{6-3} and D_{8-4}. The second type is the restricted full norm operators, where the norm is diagonal at the boundary but has a nondiagonal block in the interior. The advantage of these operators is that the order at and close to the boundary is only one order lower than in the interior, while the disadvantage is that schemes based on these operators may be unstable without the use of dissipation. The restricted full operators we use here are D_{4-3} and D_{6-5}.

If the computational domain is split into several subdomains ("patches"), the discrete representation requires a stable technique to communicate the solution at interpatch boundaries. We make use of a penalty method [29], which adds a damping term to the right hand side of the evolution equation at the boundary point in a way which retains linear stability. The method has a free parameter, called δ in Ref. [29], which determines how much the difference between characteristic fields on either side of the interpatch boundary is penalized. Different values of δ result in different amount of energy dissipation at the interpatch

boundary and can in principle be chosen so that no energy is dissipated (this is marginally stable). Usually the value of δ is chosen such that some dissipation of energy occurs. With constant values of δ the amount of dissipation decreases with resolution.

D. Numerical code

For the purposes of this paper, a one-dimensional code which supports constraint-preserving boundaries, multiple grid patches, and the use of the aforementioned high-order SBP derivative and dissipation operators has been developed. In addition, the code is able to reproduce the (single grid and without CPM matching) second-order methods of Ref. [25] for comparison. We use the methods of lines, and the time integration is performed by a 4th order Runge-Kutta method. The grid patches that we consider here are not intersecting, but touching. This implies, that each grid function is double valued at the patch interface coordinate since the SBP derivative operators are one sided at the boundaries. To ensure consistency without compromising (linear) stability, we make use of a penalty method as described above. Constraint-preserving boundary conditions require the calculation of derivatives of certain grid functions at the outer boundary, which we also obtain by using the SBP derivative operators.

In a black hole setting, the computational domain next to the excision boundary tends to quickly amplify high frequency noise, which can not be represented accurately on the discrete grid. This is especially true for high-order accurate derivative operators. Thus, high-order simulations of black holes need a certain amount of numerical dissipation to be stable. This dissipation is here provided by the SBP dissipation operators constructed in Ref. [22]. The free parameters of these operators, namely, the coefficient of the dissipation and the extent of the transition region (for nondiagonal operators), are found by numerical experiment.

III. RESULTS

The numerical experiments presented in this section are set up to systematically test the performance of the new techniques in several situations of increasing difficulty. We start with a series of tests evolving a Schwarzschild black hole in Painlevé-Gullstrand coordinates with either a single patch or two patches matched via the penalty method, and compare the performance of all SBP operators with the second-order finite-differencing method presented in [25]. Next, to test more dynamical situations, a gauge or scalar field signal is injected in a constraint-preserving manner through the outer boundary and accreted onto the black hole. A robust stability test is then performed with noise on the incoming gauge mode u_3, and, with Cauchy-perturbative matching, on the scalar field mode u_8. Finally, a series of high-precision tests involving all techniques are presented, in which a black hole accretes a

scalar field injected through the outer boundary of the perturbative patch.[4] These simulations also include a test of the long-term stability and accuracy after accretion and ring-down.

A. Schwarzschild black hole in Painlevé-Gullstrand coordinates

In our first series of tests, a Schwarzschild black hole is evolved with high-order accurate SBP operators, constraint-preserving boundary conditions and excision. Cauchy-perturbative matching is not used in these tests. To fix the coordinate system, we make use of the horizon-penetrating Painlevé-Gullstrand coordinates [27,28], and we fix the coordinate functions $\tilde{\alpha}$ and β of the previous section to their exact values.

For all tests, the inner boundary is located well inside the event horizon (more precisely, it is located at $r_e = 1M$), which implies that all modes are outflow. Therefore, no boundary conditions may be applied at the excision boundary. The exact boundary location is not crucial as long as it is inside the apparent horizon, but this choice facilitates comparison with [25]. Also, in dynamical situations the apparent horizon location may move significantly on the coordinate grid, and to ensure outflow conditions at the inner boundary some penetration into the black hole is of advantage. To match the setup of [25], we set the outer boundary to $r = 10M$. To ensure well-posedness of the continuum problem, boundary conditions should be applied to the incoming modes u_1, u_2, u_3, u_4, and u_8. However, three of these modes, namely u_1, u_2, and u_4, can be fixed by the use of constraint-preserving boundary conditions, as discussed in Sec. II, which leaves the freely specifiable gauge mode u_3 and the scalar field mode u_8. Since in these initial tests we are only interested in obtaining a stationary black hole solution, the initial scalar field is set to zero, and the (scalar field) characteristic mode u_8 is penalized to zero as well. The incoming gauge mode u_3 is penalized to the exact solution.

An error function δM can be defined by use of the Misner-Sharp mass function [1]

$$M(r) := \frac{r g_T}{2}\left[1 + \frac{r^2}{g_T}\left(K_T^2 - \frac{f_{rT}^2}{g_{rr}} \right) \right], \qquad (3)$$

where then, if the black hole's mass is denoted by M, $\delta M(r) = (M(r) - M)/M$. Since the same error measure and continuum system is used in [25], we can compare the different discrete approaches directly.

---

[4]Note that boundary conditions are used to inject a pulse into the domain. This permits to get nontrivial solutions without solving the constraints for the initial data. These outer boundary conditions are nonphysical in the sense that we are injecting waves, not extracting them.

1. One grid patch

The computational domain $r \in [1, 10]$ is represented by one coordinate patch, which is exactly the same setup as in Ref. [25]. In Fig. 1 we compare for coarse and high resolutions, $\Delta r = M/8, M/64$, the performance of the methods used in Ref. [25], namely, second-order spatial derivatives with fourth order Kreiss-Oliger dissipation (which is set to zero near the boundaries) and a third order extrapolation at the boundaries, with the SBP derivative and dissipation operators D_{2-1}, D_{4-2}, D_{4-3}, D_{6-3}, D_{6-5} and D_{8-4}. The figure shows the evolution of the L_2 norm of the Misner-Sharp mass error over an evolution time of $10,000M$. In all cases displayed there is a linear growth in the error after some time. This is an artefact of the discrete representation of the constraint-preserving bound-
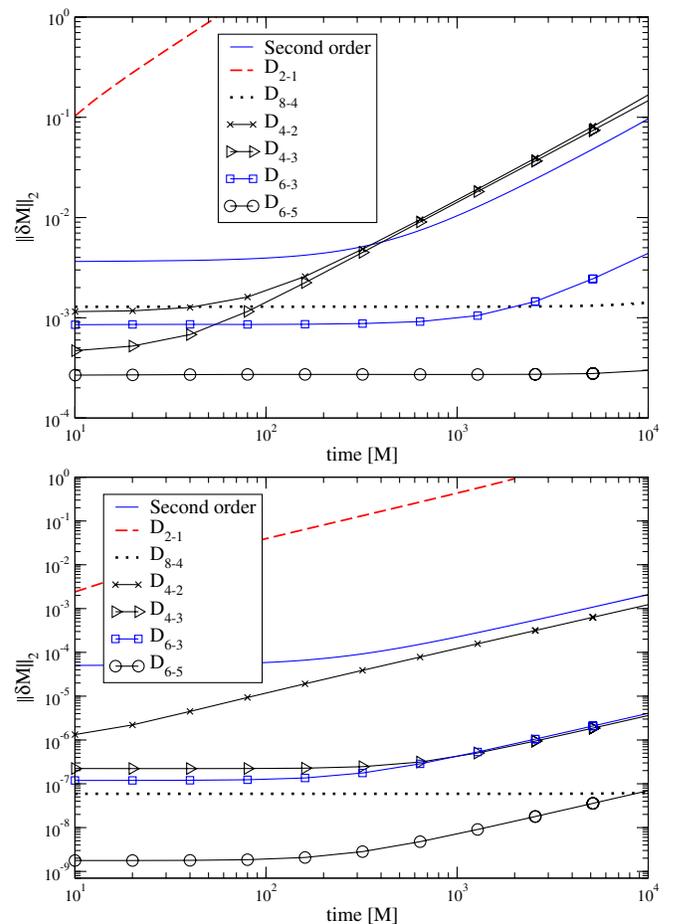

FIG. 1 (color online). Time evolution of the relative error in the Misner-Sharp mass function when evolving a Schwarzschild black hole in Painlevé-Gullstrand coordinates with one grid patch, for different discrete methods. Two resolutions are displayed, corresponding to $\Delta r = M/8$ (upper panel) and $\Delta r = M/64$ (lower panel). The result from the method presented Ref. [25] is denoted by ''second order'', while new results are marked by the SBP derivative and dissipation operators used. The high-order operators D_{6-5} and D_{8-4} display superior performance already at the lowest resolution.

ary conditions. We have also performed tests with maximally dissipative boundary conditions: these yield a discrete equilibrium after some time, and thus allow for evolutions of unlimited time. However, since these boundary conditions are not correct for most systems of practical interest, we only make use of this result to point out the source of the linear growth of errors observed, which converges away with increasing resolution.

As soon as the error gets close to 1, the code encounters an instability, which, in this case, is associated with a migration of the excision boundary outside of the black hole, and consequently ill-posedness of the continuum problem. While this migration could be theoretically avoided by choosing horizon-fixing dynamical coordinate conditions, a solution with this magnitude of error is, in any case, not of practical use.

In the present numerical code, the SBP operators are also used as one-sided derivatives for determining the constraint-preserving boundary conditions, which suggests that the operator D_{2-1}, which is only first order at the boundaries, will yield less accurate outer boundary conditions than the third order method in [25]. Figure 1 clearly demonstrates this fact. However, the operators D_{6-3}, D_{6-5} and D_{8-4} are significantly more accurate than the results presented in Ref. [25], and already so at the coarsest resolution. Furthermore, at $\Delta r = M/64$ the SBP operator D_{6-5} induces a solution error of less than 10^{-7} (that is, *four orders of magnitude smaller than the corresponding errors when using the second-order method of* [25] *with the same resolution*) within 10,000M, which appears sufficiently accurate for many practical purposes.

The long-term evolution of a Schwarzschild black hole with the operators D_{6-5} and D_{8-4} is displayed in Fig. 2. The linear growth of errors dominates the solution at late
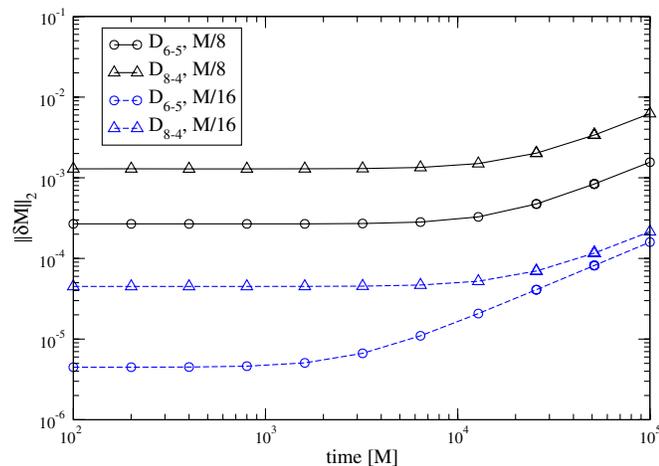
times, but since this error significantly decreases with resolution, long evolution times can be obtained even for moderate radial grid spacings. This is naturally an interesting feature for simulations with three-dimensional spatial grids, where computational resources are still a viable concern.

2. Two grid patches

As dicussed in the introduction, the use of multiple coordinate patches has advantages when modelling black holes. To implement a stable interface boundary condition, the penalty method is used to ensure linear stability. Here we first investigate the performance of the SBP operators coupled to an interpatch penalty boundary method by evolving a black hole spacetime covered by two noninter-
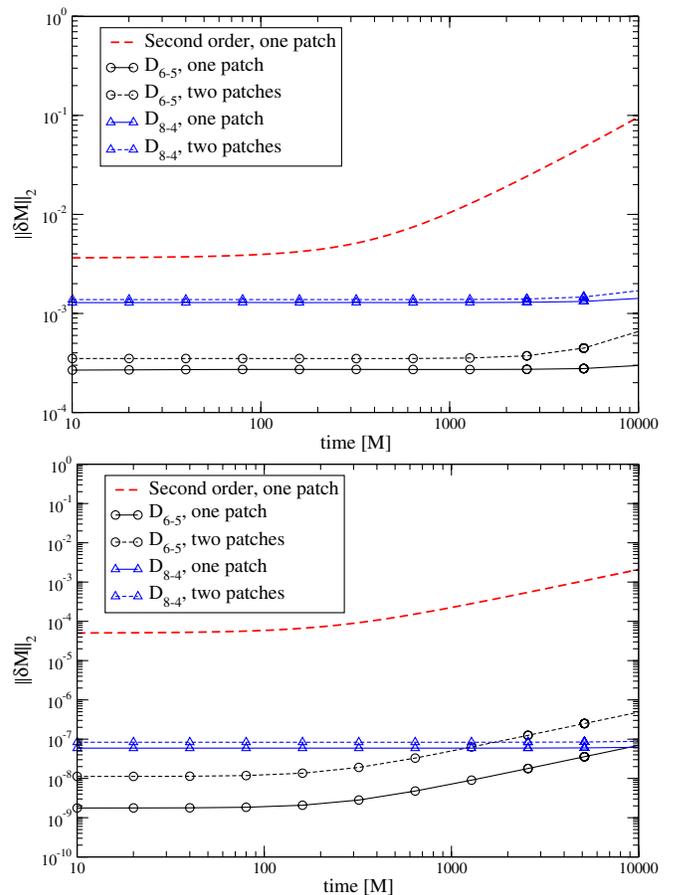

FIG. 3 (color online). Comparison of unipatch and multipatch evolutions of a Schwarzschild black hole in Painlevé-Gullstrand coordinates. The graphs denoted by ''one patch'' and ''second order'' are those from Fig. 1, while the corresponding graphs for ''two patches'' cover the computational domain with two nonintersecting spherical shells, the first one from $r = 1M$ to $r = 5.5M$, and the second one from $r = 5.5M$ to $r = 10M$. The one-sided derivatives at the interface boundary introduce a very small loss of accuracy. In the upper and lower panels the resolution is $\Delta r = M/8, M/64$, respectively. For the late time behavior of D_{6-5} and D_{8-4} please also cf. Figure 2.

FIG. 2 (color online). Evolution of a Schwarzschild black hole for 100,000M. The axes show the quantities described in Fig. 1. It is clear that even with low resolutions of $\Delta r = M/8$ and $M/16$, the operators D_{6-5} and D_{8-4} are able to evolve the black hole in a stable manner for a significant time.
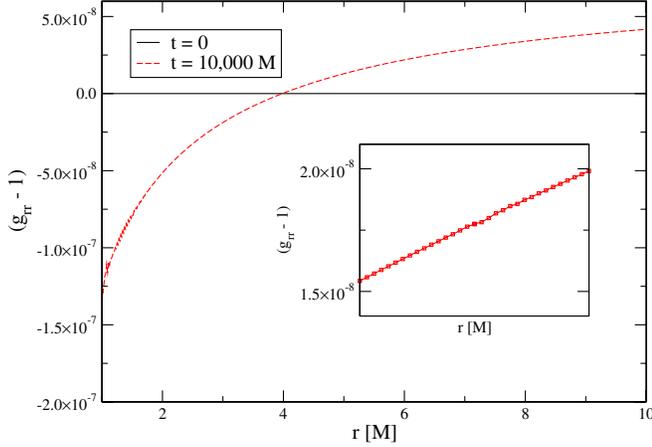
FIG. 4 (color online). Evolution of metric function g_{rr} for a black hole in Painlevé-Gullstrand coordinates, with a resolution of $\Delta r = M/64$, two grid patches with an interface at $r = 5.5M$ and using the SBP operator D_{6-5}. The two graphs show the metric function at $t = 0$ (where $g_{rr}(r) = 1$) and at $t = 10,000M$. The inset shows the region around the interface between the grid patches.

secting spherical shells, the first one from $r = 1M$ to $r = 5.5M$, and the second one from $r = 5.5M$ to $r = 10M$. In order to provide an intermediate test towards the CPM tests below, we do a nonlinear matching, communicating all characteristic modes (that is, without imposing for the moment constraint-preserving boundary conditions at the matching interfaces).

The free parameter of the penalty boundary condition δ introduced in section II C is set to the dissipative value 0. Only the operators D_{6-5} and D_{8-4} are used for comparison to the results from the previous section.

In Fig. 3 the performance of the multipatch system is compared to the unipatch results from the previous section. As expected, the use of one-sided derivatives at the interpatch boundary reduces the total level of accuracy, but only by a very small amount; furthermore, the system is still stable and convergent. The time of the onset of the linear growth observed in all evolutions varies between the grid setups and choices of discrete operator. Figure 4 shows the 3-metric component $g_{rr}(r)$ at the times $t = 0$ and $t = 10,000M$. The region around the interpatch interface at $r = 5.5M$ is shown in the inset, which demonstrates that the penalty method introduces no strong visible artifacts in this part of the solution. This observation also holds for the other solution functions.

B. Gauge wave on a Schwarzschild background

The next series of tests focuses on a dynamical situation, namely, the evolution of a Schwarzschild black hole in nonstationary coordinates. For this purpose, the initial data is set to a Schwarzschild black hole in Painlevé-Gullstrand coordinates as in Sec. III A, as is the lapse and shift function at all times, but the incoming gauge mode u_3 at

the outer boundary is set to a Gaussian pulse of the form

$$u_3(t) = u_3^{\text{PG}}(1 + Ae^{-(t-t_0)^2/\tilde{\sigma}^2}). \tag{4}$$

Here, u_3^{PG} is the exact gauge mode from the stationary solution. As in Ref. [25], we impose a strong pulse with $A = 1$, $t_0 = 5M$ and $\tilde{\sigma} = 2M$. Since the solution is now not adapted to the asymptotically timelike Killing field, the SBP operators and multipatch techniques can be tested on a solution with wave propagation without compromising the use of the error measure $||\delta M||_2$. To facilitate comparison with Ref. [25], the outer boundary is located at $r = 30M$ in these tests.

Figure 5 shows results from the gauge pulse problem on a single grid patch and two grid patches, here with an interpatch boundary at $r = 15.5M$. While in the stationary
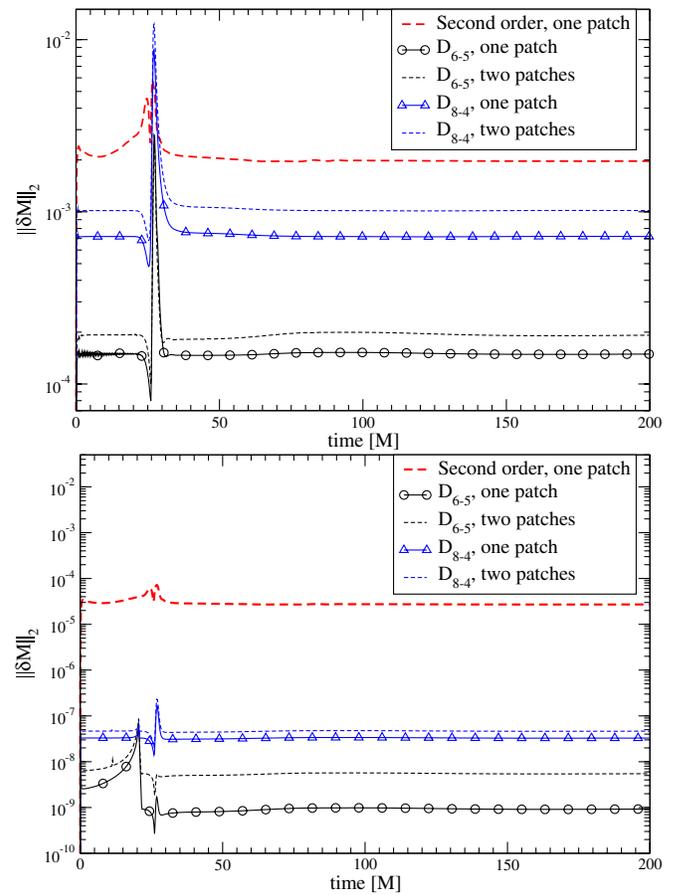

FIG. 5 (color online). Comparison of unipatch and multipatch evolutions of a gauge wave travelling on a Schwarzschild background. The graphs denoted by ''second order'' are obtained with the methods in Ref. [25], while the corresponding graphs for ''one patch'' and ''two patches'' cover the computational domain with either one or two nonintersecting spherical shells, the first one from $r = 1M$ to $r = 15.5M$, and the second one from $r = 15.5M$ to $r = 30M$. The one-sided derivatives at the interface boundary introduce a small loss of accuracy, but the system is still stable. The upper and lower panels correspond to $\Delta r = M/8$ and $M/64$, respectively.

case the interpatch boundary method only had to deal with small numerically introduced differences between the values of the geometrical quantities at the interface, the nonstationary case introduces a large pulse travelling over the boundary, and is thus a much more severe test for accuracy and stability of the penalty method. The solution error is dominated by the ability of the discrete method to represent the propagation and accretion of the gauge pulse, and by possible artefacts introduced by the interpatch boundary.

Judging from Fig. 5, the high-order operators are stable and significantly more accurate than a second-order method also in a dynamical situation, and even when using multiple matched domains.

C. Accretion of a scalar field pulse

Since the outer boundary has two free incoming modes, it is possible to inject a scalar field pulse in a way similar to the gauge pulse of Sec. III B. In contrast to the gauge pulse, however, this system will result in an increase of the mass of the black hole, which also implies that the Misner-Sharp mass cannot be used as a measure of the errors anymore. A possible choice for a gauge field source with compact support is

$$
u_8(t) = \begin{cases} 0 & t < t_I \\ \frac{A}{t_F^8}(t - t_I)^4(t - t_F)^4 \sin\left(\frac{\pi t}{t_F}\right) & t \in [t_I, t_F] \\ 0 & t > t_F \end{cases}
$$

To facilitate comparisons with Ref. [25] we use an amplitude $A = 7.2$, and $t_I = 0M$, $t_F = 10M$ and set the computational domain to be $r \in [1, 50]M$.

For resolutions $\Delta r = M/20$ and $\Delta r = M/40$, the time evolution of the apparent horizon is shown in Fig. 6. The scalar pulse leads to a significant increase of the black hole
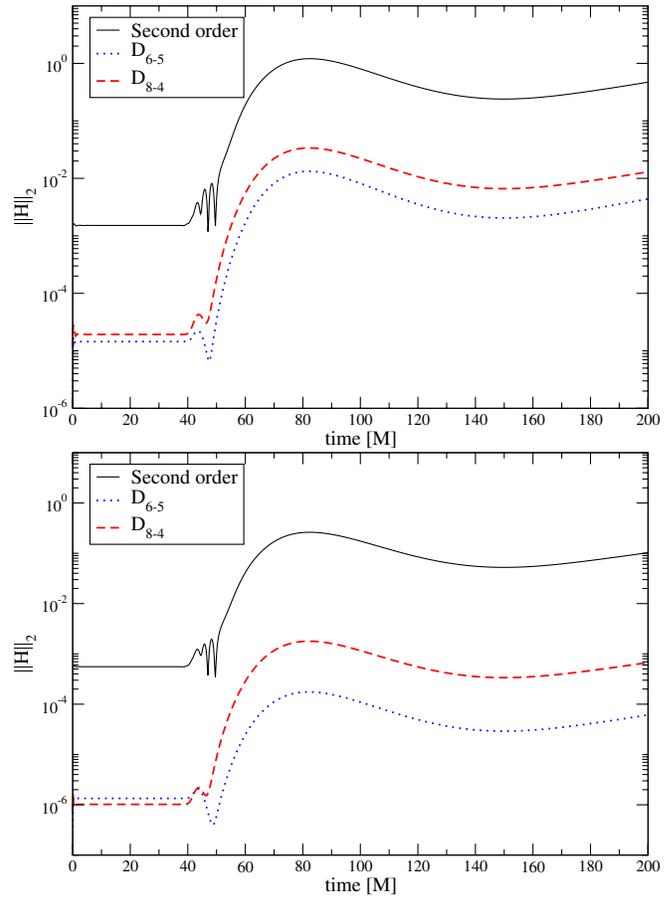

FIG. 7 (color online). L_2 norm of the Hamiltonian constraint over time for the accretion of a strong scalar field pulse to a Schwarzschild black hole, with resolutions $\Delta r = M/20$ and $M/40$ (upper and lower panels, respectively). The graph denoted by "second order" is obtained with the method presented in [25], and the D_{6-5} and D_{8-4} are obtained using the corresponding SBP operators.

FIG. 6 (color online). Evolution of the apparent horizon mass for the accretion of a strong scalar pulse to a Schwarzschild black hole. Shown are plots for two resolutions, $\Delta r = M/20$ and $\Delta r = M/40$, using the SBP operator D_{6-5}. The large scalar field amplitude leads to a significant increase in the black hole mass.
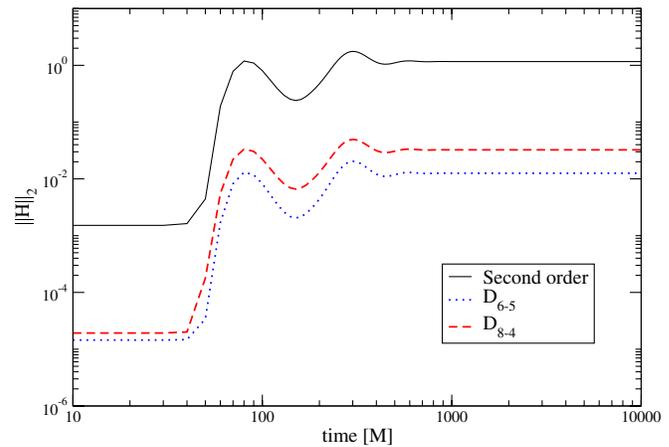

FIG. 8 (color online). As Fig. 7, but evolved for $10,000M$ with $\Delta r = M/20$ to demonstrate the long-term behavior after accretion of the pulse.
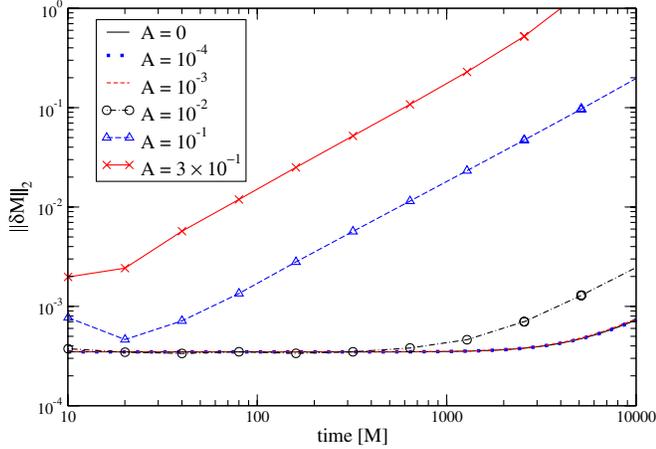
FIG. 9 (color online). Results of a robust stability test for different random noise amplitudes. The system is a Schwarzschild black hole in Painlevé-Gullstrand coordinates, and the computational domain $r \in [1, 10]M$ is covered by two patches with a boundary at $r = 5.5M$ and a resolution of $M/8$. Random noise is superimposed on the ingoing gauge mode u_3, with an amplitude denoted by A. The graphs show the mass error with time for different random noise amplitudes, obtained with the SBP operator D_{6-5}.

mass by a factor of ≈ 2.7 after the pulse is inside the black hole. Larger amplitudes are not obtainable with the simple gauge prescription used here, but a horizon-freezing gauge condition could improve on this result. As a replacement for the Misner-Sharp error measure, we plot the L_2 norm of the Hamiltonian constraint over time in Fig. 7. It is apparent that the high-order operators are again stable and more accurate than the second-order operator. The graphs indicate a growth of the constraint near $t = 200M$, but a long-term evolution with $\Delta r = M/20$ shown in Fig. 8 demonstrates that the system settles down to stability after the accretion.

D. Robust stability test with gauge noise

The term *robust stability test* [30,31] typically refers to the discrete stability of a numerical system in response to random perturbations. In this case, we will use the same system as in Sec. III A 2, but impose random noise on the incoming gauge mode u_3 with a certain amplitude. To test the discrete stability of the evolution system, we chose a large range of amplitudes from 10^{-4} to 0.3. Random perturbations of the latter amplitude is significant for a nonlinear system.[5]

For this multipatch test, results in the mass error for a resolution $\Delta r = M/8$ are shown in Fig. 9. It is apparent

---

[5]Beyond this amplitude the inner boundary tends to become partially inflow by moving the apparent horizon beyond the computational domain. More sophisticated gauge or inner boundary condition could alleviate this, but since we are interested here in a proof of principle, a simple system is preferred.
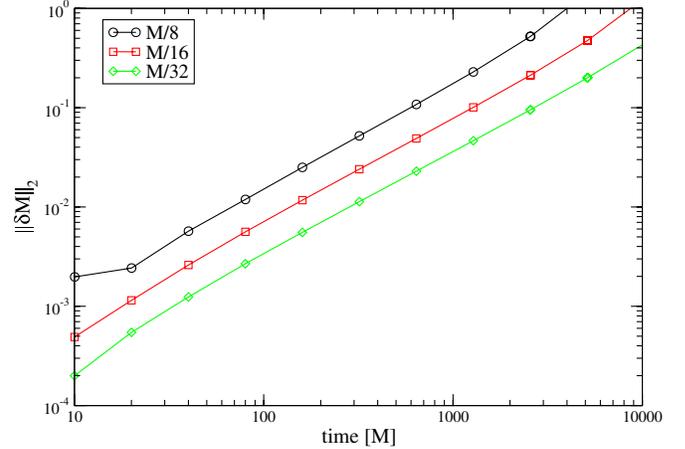

FIG. 10 (color online). Like Fig. 9, but for the highest random noise amplitude 0.3 and different resolutions.

that strong random noise induces a stronger growth in the solution error. However, this growth is still linear. As in all black hole evolutions in Sec. III A, the system encounters a numerical instability as the solution error approaches 1, but this is not a consequence of the random noise, but of the inner boundary becoming partially inflow due to a coordinate motion of the apparent horizon. Also, with increasing resolution, the growth rate of the error does not increase, as shown in Fig. 10. We conclude that this high-order evolution system is discretely stable against strong random perturbations.

E. Cauchy-perturbative matching: robust stability test with scalar field noise

We now test the stability of the system with Cauchy-perturbative matching against random perturbations in the scalar field. To this end, the computational domain is again subdivided as in Sec. III D, but the right patch evolves the scalar field on a fixed Painlevé-Gullstrand background as explained in the introduction. The interpatch boundary is thus matching the Cauchy patch to a perturbative one, and we test the stability of the system against random perturbations by imposing random noise on the incoming scalar field mode on the outer boundary of the perturbative patch.

Since the mass error is not available for a system accreting a scalar field, the L_2 norm of the Hamiltonian constraint is used again in Fig. 11. No exponential growth can be observed in the Hamiltonian constraint violation. The same is true when increasing the resolutions, as in Fig. 12, which also deserves some additional comments: The robust stability test does not lead to a converging sequence of solutions if the random noise amplitude is not diminished with resolution. However, the purpose of these tests is to excite any unstable high frequency modes present in the numerical system. The absence of any mode growing with increasing resolution shows that the system with a Cauchy-perturbative matching interface is stable even against
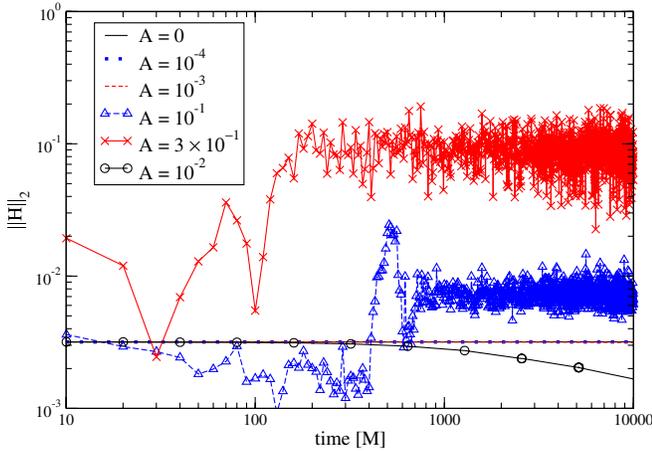
FIG. 11 (color online). Robust stability test with Cauchy-perturbative matching. The system is a dynamically evolved Schwarzschild black hole in Painlevé-Gullstrand coordinates matched to a perturbative module at $r = 5.5M$ as described in the introduction. Random noise is imposed via the incoming scalar field mode at the outer boundary. Plotted is the L_2 norm of the Hamiltonian constraint over time for different noise amplitudes. All evolutions were done with a resolution of $\Delta r = M/8$ and the SBP operator D_{6-5}.
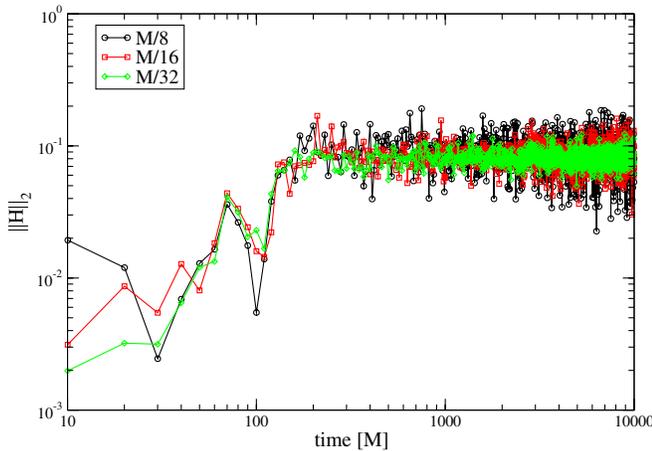
FIG. 12 (color online). Like Fig. 11, but for the highest random noise amplitude and different resolutions.

strong random noise injected into the system. This is a promising result for any effort to do three-dimensional matching between Cauchy modules and perturbative ones using multiple patches and high-order summation-by-parts operators.

F. Cauchy-perturbative matching: Accretion of a "gravitational wave" and long-term evolution

Finally, using the massless Klein-Gordon field as a scalar analogue of gravitational waves in spherical symmetry, we model the accretion of a gravitational wave packet across a Cauchy-perturbative matching boundary.
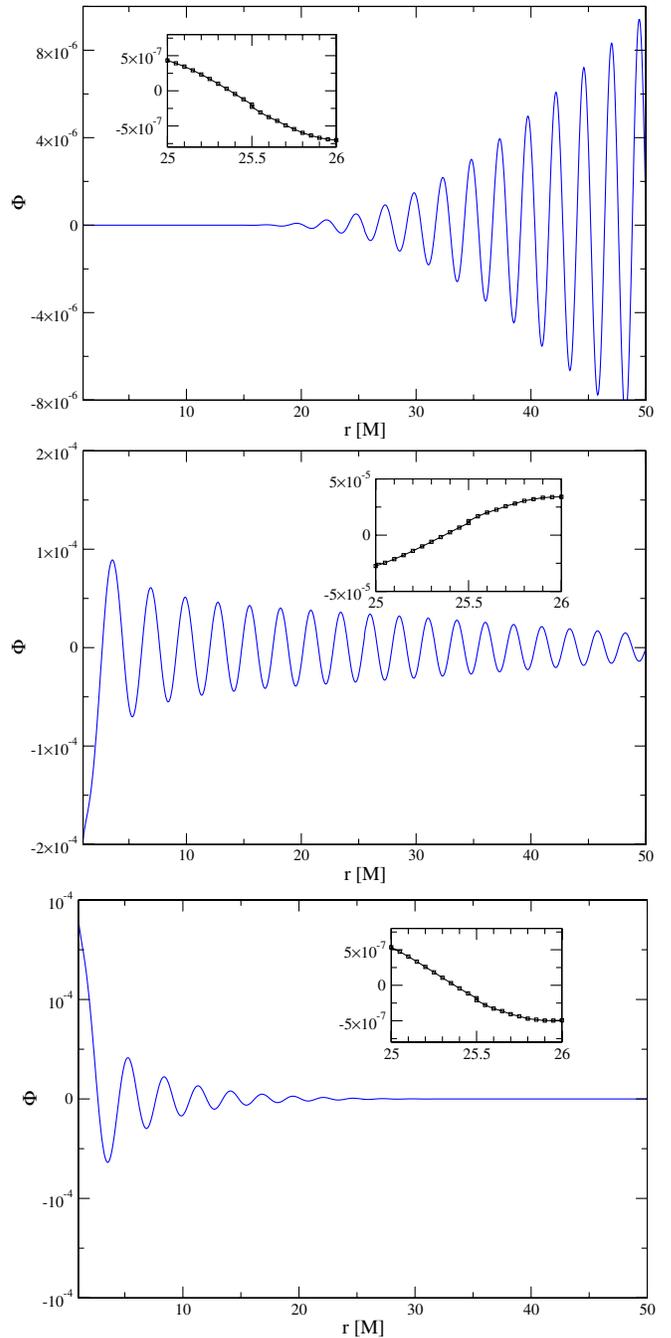

FIG. 13 (color online). Accretion of a scalar wave packet across a Cauchy-peturbative matching interface, as a scalar analog for gravitational wave accretion in three-dimensional simulations. The packet consists of 50 waves injected from $t = 0$ to $t = 100M$, as described in the text. Here, the grid function Φ is plotted over the radial coordinate at $t = 30M$, $65M$, $110M$ (from top to bottom), for the resolution $\Delta r = M/20$ and the SBP operator D_{6-5}. The inset shows the behavior of the grid function around the matching interface, which is at $r = 25.5M$. Note that even though the grid function is in principle two-valued on the interface, the penalties in conjunction with high-order operators only lead to a very small mismatch.
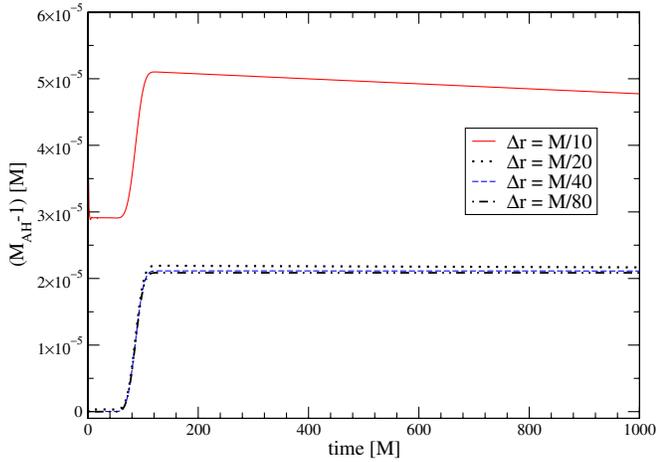
FIG. 14 (color online). Accretion of a scalar wave packet across a Cauchy-peturbative matching interface. This plot shows the apparent horizon mass over time for evolutions with different resolutions and the SBP operator D_{6-5}.

This test is an extension of the single-patch scalar field accretion of Sec. III C, and makes use of all ingredients presented in this paper for a stable and accurate evolution of black holes with Cauchy-perturbative matching.

Since Cauchy-perturbative matching assumes the gravitational wave to be a small perturbation of a fixed background in the wave zone, the amplitude of the wave packet that we inject through the outermost boundary is chosen to be $A = 0.01$. Similarly to section III C, we describe the packet by the function

FIG. 15 (color online). Accretion of a scalar wave packet across a Cauchy-peturbative matching interface. This plot shows the L_2 norm of the Hamiltonian constraint for different resolutions, using the SBP operator D_{6-5}. *The nonlinear constraint violations introduced at the continuum by the matching are small enough that they cannot be detected in these very accurate simulations.* Please note, for comparison with Fig. 8, that the amplitude of the Klein-Gordon signal is smaller compared to Sec. III C.

FIG. 16 (color online). Accretion of a scalar wave packet across a Cauchy-peturbative matching interface. To demonstrate the advantage of using high-order methods, $(M_{AH} - 1)$ is shown for evolutions obtained with the SBP operators D_{4-3} D_{6-5}, with resolution $\Delta r = M/10$. The loss of mass after accretion of the wave packet with compact support in $t \in [0 100] M$ is a numerical artefact, which converges away with resolution. The inset shows that the evolution obtained with the operator D_{4-3} is not unstable, but only significantly less accurate.

$$u_8(t) = \begin{cases} 0 & t < t_I \\ \dfrac{A}{t_F^8}(t - t_I)^4 (t - t_F)^4 \sin(\frac{\pi t}{n t_F}) & t \in [t_I, t_F] \\ 0 & t > t_F \end{cases}$$

where for the number of half waves in the pulse we set $n = 100$. We inject the packet from $t_I = 0$ to $t_F = 100M$. The plots in Fig. 13 display the the evolution of the grid function Φ, and specifically the behavior of the function around the Cauchy-perturbative matching interface, which is at $r = 25.5M$. The corresponding increase in apparent horizon mass is shown in Fig. 14. The evolution of the Hamiltonian constraint violation using the SBP operator
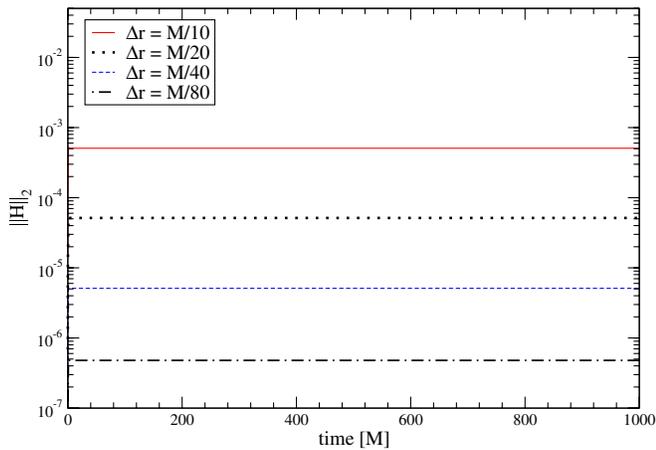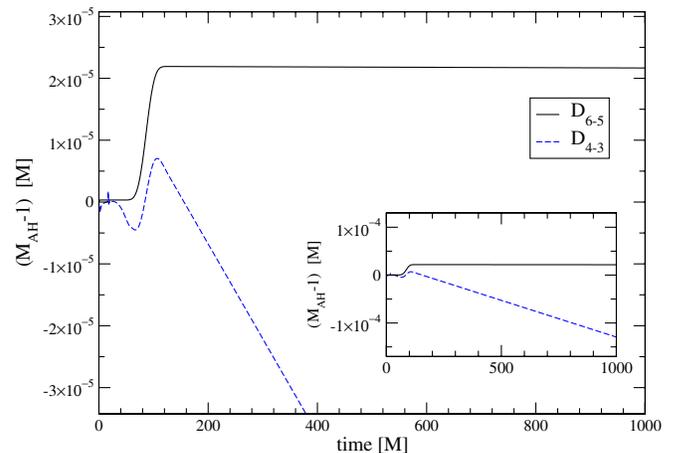

FIG. 17 (color online). Like Fig. 16, but for a resolution of $\Delta r = M/20$.

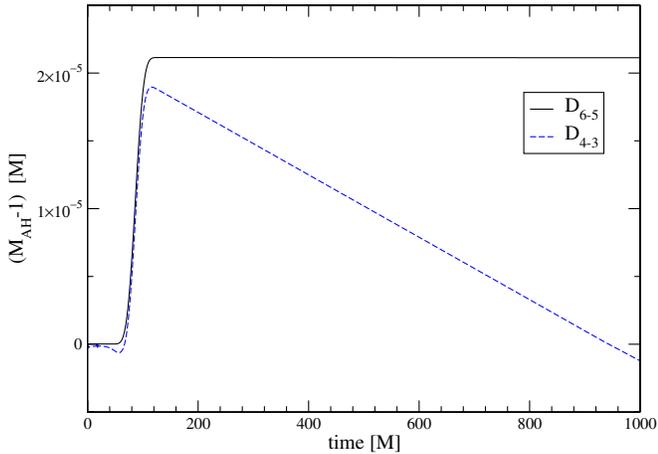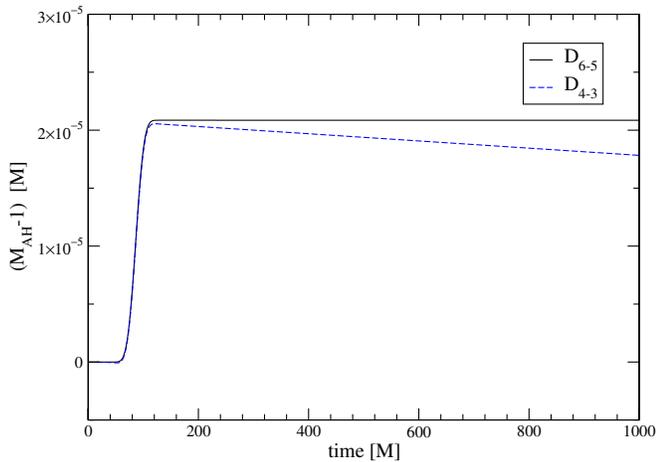FIG. 18 (color online). Like Fig. 16, but for a resolution of $\Delta r = M/40$.

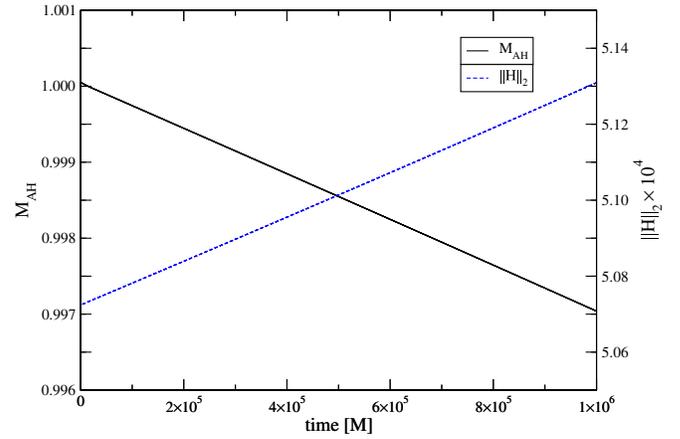FIG. 19 (color online). Like Fig. 16, but for a resolution of $\Delta r = M/80$.

FIG. 20 (color online). Long-term stable evolution of a Schwarzschild black hole after accretion of a scalar wave packet with Cauchy-perturbative matching. The SBP operator D_{6-5} is used with a resolution of $\Delta r = M/10$. Plotted are the apparent horizon mass and the Hamiltonian constraint over time. The apparent horizon mass indicates that the discrete evolution introduces a relative error of about 0.3% after $1,000,000M$.

D_{6-5} and different resolutions is shown in Fig. 15. It is apparent that with the techniques used not only is the discrete system stable and accurate, *but also the amount of nonlinear constraint violations introduced at the continuum by the Cauchy-perturbative matching are very small*, in Fig. 15 they must actually be smaller than 10^{-6}.

The advantages of using high-order methods is made evident in Figs. 16–19. In these plots, the performance of the SBP operator D_{6-5}, which is sixth order in the interior and fifth order at the boundaries, is compared to that of the operator D_{4-3}, which is fourth order in the interior and third order at the boundaries, for different choices of resolution. Although both operators show convergence, for a mass increase of about 10^{-5}, the operator D_{4-3} is unable to reproduce the correct behavior with reasonable grid resolutions. We consider this specifically important for three-dimensional simulations, where the necessary resources scale with n^4 if n denotes the number of grid points

in each direction. Thus, for all simulations requiring a certain amount of precision, high-order operators are an essential requirement.

The long-term evolution of a Schwarzschild black hole accreting a wave packet over a Cauchy-perturbative matching interface and settling down to equilibrium is shown in Fig. 20. The black hole is evolved for $1,000,000M$ with the lowest resolution $\Delta r = M/10$ and the SBP operator D_{6-5}. While an evolution of this length might appear to be of only technical interest, we note that modelling phenomena like hypernovae and collapsars in general relativity will require the stable evolution of a black hole for at least several seconds, which is the lower end of timescales associated with the collapsar model of gamma-ray burst engines [32]. For a stellar mass black hole, $M = M_\odot \approx 5\,\mu s$, that is $1s \approx 200\,000M_\odot$.

IV. CONCLUSIONS AND OUTLOOK

To obtain long-term evolutions of compact astrophysical systems in three spatial dimensions, advanced numerical techniques are preferable in that they may improve stability and accuracy of the associated discrete model system. While high accuracy enables efficient use of the available computational resources, well-posedness of the continuum model and numerical stability are requirements which can not be met by increasing computational power. A number of techniques have been suggested to address these issues [29]: Multiple coordinate patches, typically adapted to approximate symmetries of certain solution domains, combined with high-order operators are expected to increase the accuracy of any model of a stellar system. Cauchy-perturbative matching provides an efficient way to accurately model the propagation of gravitational waves to a

distant observer, and to yield physical boundary conditions on incoming modes of the Cauchy evolution. Constraint-preserving boundary conditions isolate the incoming modes on the constraint hypersurface, and, finally, for evolving black holes, an excision boundary is desirable to concentrate on the behavior of the external spacetime. Only recently the consideration of the well-posedness of the differential system and the application of theorems on discrete stability of the numerical system have provided hints as how to address the outstanding issues. In this paper, we have applied all these techniques to a model system: a spherically symmetric black hole coupled to a massless Klein-Gordon field.

We find that the use of a first-order hyperbolic formulation of Einstein's field equations, combined with high-order derivative and dissipation operators with the summation-by-parts property, penalized interpatch boundary conditions and constraint-preserving outer boundary conditions leads to a stable and accurate discrete model. Specifically, isolated Schwarzschild black holes in coordinates adapted to the Killing fields, and in coordinates on which a gauge wave is imposed, and Schwarzschild black holes accreting scalar wave pulses were taken as typical model systems involving excision. The results show that the introduction of several coordinate patches and of a Cauchy-perturbative matching interface does not introduce significant artefacts or instabilities. Rather, the high-order methods allow the accurate long-term evolution of accreting black holes with excision and Cauchy-perturbative matching in reasonable resolutions. As an example, we have presented the evolution of such a system with the high-order SBP operator D_{6-5}, which, at a resolution of $\Delta x = M/10$, introduced an error of only 0.3% after an evolution time of $1,000,000M$.

Most systems of interest in general relativistic astrophysics will necessarily require the use of three-dimensional codes. Results from a one-dimensional study are useful in that (i) experience can be gained in a clean but nontrivial physical system, (ii) they can be easily reproduced without the need for implementation of three-dimensional codes with multiple coordinate patches and (iii) isolation of sources of difficulty in the three-dimensional setting can be obtained more easily. With the promising results from this study, we will, as a next step, apply these techniques to a three-dimensional general relativistic setting.

[1] C. W. Misner, K. S. Thorne, and J. A. Wheeler, *Gravitation* (W. H. Freeman, San Francisco, 1973).
[2] T. Regge and J. Wheeler, Phys. Rev. **108,** 1063 (1957).
[3] F. J. Zerilli, Phys. Rev. Lett. **24,** 737 (1970).
[4] L. Lehner, O. Reula, and M. Tiglio Class. Quant. Grav. **22,** 5283 (2005).
[5] J. Thornburg, Class. Quant. Grav. **21,** 3665 (2004).
[6] L. E. Kidder, M. A. Scheel, and S. A. Teukolsky, Phys. Rev. D **64,** 064017 (2001).
[7] S. R. Lau, J. Math. Phys. (N.Y.) **46,** 102503 (2005).
[8] J. Winicour (to be published).
[9] N. T. Bishop, R. Gómez, L. Lehner, and J. Winicour, Phys. Rev. D **54,** 6153 (1996).
[10] R. Gómez, R. L. Marsa, and J. Winicour, Phys. Rev. D **56,** 6310 (1997).
[11] L. Rezzolla, A. M. Abrahams, R. A. Matzner, M. E. Rupright, and S. L. Shapiro, Phys. Rev. D **59,** 064001 (1999).
[12] M. E. Rupright, A. M. Abrahams, and L. Rezzolla, Phys. Rev. D **58,** 044005 (1998).
[13] R. Gómez, L. Lehner, R. Marsa, J. Winicour, A. M. Abrahams, A. Anderson, P. Anninos, T. W. Baumgarte, N. T. Bishop, and S. R. Brandt *et al.,* Phys. Rev. Lett. **80,** 3915 (1998).
[14] A. M. Abrahams, L. Rezzolla, M. E. Rupright, A. Anderson, P. Anninos, T. W. Baumgarte, N. T. Bishop, S. R. Brandt, J. C. Browne, and K. Camarda *et al.,* Phys. Rev. Lett. **80,** 1812 (1998).
[15] O. Sarbach and M. Tiglio, Phys. Rev. D **64,** 084016 (2001).
[16] O. Sarbach and M. Tiglio, gr-qc/0412115.
[17] L. E. Kidder, L. Lindblom, M. A. Scheel, L. T. Buchman, and H. P. Pfeiffer, Phys. Rev. D **71,** 064020 (2005).
[18] B. Szilagyi and J. Winicour, Phys. Rev. D **68,** 041501(R) (2003).
[19] B. Strand, J. Comput. Phys. **110,** 47 (1994).
[20] B. Strand, Ph.D. thesis, Uppsala University, 1996.
[21] K. Mattsson, M. Svärd, and J. Nordström, J. Sci. Comput. **21,** 57 (2004).
[22] P. Diener, E. N. Dorband, E. Schnetter, and M. Tiglio

(unpublished).

[23] A. Anderson and J. W. York, Phys. Rev. Lett. **82**, 4384 (1999).

[24] L. E. Kidder, M. A. Scheel, S. A. Teukolsky, E. D. Carlson, and G. B. Cook, Phys. Rev. D **62**, 084032 (2000).

[25] G. Calabrese, L. Lehner, and M. Tiglio, Phys. Rev. D **65**, 104031 (2002).

[26] P. Painlevé, C.R. Acad. Sci. **173**, 677 (1921).

[27] A. Gullstrand, Ark. Mat. Astron. Fys. **16**, 1 (1922).

[28] K. Martel and E. Poisson, Am. J. Phys. **69**, 476 (2001).

[29] L. Lehner, O. Reula, and M. Tiglio, gr-qc/0507004.

[30] B. Szilágyi, R. Gómez, N. T. Bishop, and J. Winicour, Phys. Rev. D **62**, 104006 (2000).

[31] M. Alcubierre *et al.*, Class. Quant. Grav. **21**, 589 (2004).

[32] A. I. MacFadyen, S. E. Woosley, and A. Heger, Astrophys. J. **550**, 410 (2001).